MANUSCRIPT TITLE

3D-super-enhancers are condensate-associated cis-regulatory communities

AUTHORS

Jie Lv[1]†, Kelsey A. Maher[1]†, Li Dong[1], Virginia Valentine[2], Alaguraj Veluchamy[1], Tilley Tian[1], Yuna Kim[1], Bensheng Ju[1], Marc Valentine[2], John Easton[1], Steven Burden[2], Stanley B. Pounds[3], and Brian J. Abraham[1]*

[1]St. Jude Children's Research Hospital, Department of Computational Biology, Memphis, TN, 38105, USA.
[2]St. Jude Children's Research Hospital, Cytogenetics Shared Resource, Memphis, TN, 38105, USA.
[3]St. Jude Children's Research Hospital, Department of Biostatistics, Memphis, TN, 38105, USA.

* To whom correspondence should be addressed. Email: brian.abraham@stjude.org

†Jie Lv, Kelsey Maher contributed equally to this work

ABSTRACT

Transcription proteins are concentrated at nuclear transcriptional condensates. These condensates contain cis-regulatory elements (CREs), including enhancers and promoters, that are thought to regulate genes in the same condensate. The roles of condensates are of great current interest, but research into their function is limited by an inability to comprehensively identify their associated CREs. Here, we present a conceptual framework and algorithm, BOUQUET, for integrating genome topology, chromatin occupancy, and graph theory to associate CREs and transcription protein machinery with target genes and identify exceptionally protein-rich communities that interact with condensates. BOUQUET uncovers surprising quantitative correlations between community protein accumulation and gene expression phenotypes by combining accurate CRE-gene assignment with co-activator binding profiles. A small subset of communities, which we call "3D-super-enhancers," is exceptionally protein-rich. BOUQUET-predicted 3D-SEs are comparable in number to co-activator nuclear puncta, and all genes known to interact with co-activator condensates in embryonic stem cells are within 3D-SEs. 3D-SEs are enriched for association with cell identity

genes across mammalian tissues. Microscopy analyses show frequent co-localization and co-expression of genes from the same 3D-SE within a single co-activator punctum, suggesting 3D-SE components interact with co-activator condensates. Thus 3D-SEs correspond to co-activator puncta, which nominates additional condensate-associated genes and CREs.

INTRODUCTION

Gene transcription is regulated through physical interactions among cis-regulatory elements (CREs) [e.g. enhancers and promoters], their bound proteins [e.g. transcription factors (TFs), co-activators, and RNA Polymerase II (Pol II)], and one or more target genes. Several critical transcription-regulating proteins have been observed to form nuclear bodies alternately called clusters, foci, droplets, puncta, or condensates, suggesting that dense nuclear protein accumulations are mechanistically critical for the regulation of transcription (1–3). For brevity, we use the term "condensate" and intend it to mean protein-dense, membraneless, nuclear puncta with internal environments that are distinct from the surrounding nucleoplasm, though we recognize the importance of ongoing work that probes the biophysical mechanisms of these partially divergent models. Condensates can contain high concentrations of a variety of biomolecules, including Pol II, TFs, cofactors, and chromatin regions that each facilitate gene control. However, precisely which genes associate with which types of condensate, how protein-bound chromatin regions interact with condensates, and how transcriptional products are produced by condensates remain obscured. To date, individual condensates and the genes that physically associate with them have been primarily examined using single-gene microscopy case studies (4–12). Here, we propose that an approach utilizing integrative omics analyses can identify distinct sets of spatially interacting, protein-bound CREs that elucidate the transcriptional regulatory relationships among chromatin regions and their bound protein apparatus.

The few genes that have been experimentally verified to associate with transcriptional condensates are genomically proximal to domains with very high levels of co-activator binding, suggesting that accumulation of co-activator signal at relevant CREs has some degree of correlation to nuclear co-activator puncta. (4–7, 9). To this end, co-activator ChIP-seq has been used to identify super-enhancers (SEs), i.e., linearly assembled enhancer sets with exceptionally high co-activator signal, but SEs are only somewhat informative for detecting condensate-associated chromatin regions (13). Among their drawbacks, SEs only

assemble genomically proximal enhancers, and these assembled enhancer domains are assigned only to their single most proximal gene (13–15). This process fails to incorporate the important regulatory contributions of genome organization on gene expression, including long-distance enhancer-promoter interactions, insulated chromatin loops (e.g. insulated neighborhoods) that constrain and/or facilitate such interactions, the ability of other types of CREs to act as enhancers, or the complexity of densely interconnected gene-CRE regulatory networks (e.g. chromatin hubs, clusters, or cliques) (16–38). Further, when studied in mESCs, the number of linear SEs differs from the number of observed co-activator puncta by several fold (4, 13, 14, 39). Thus, even if assuming all SEs form co-activator condensates, the genomic elements affiliated with the majority of co-activator condensates remain unknown.

In this study, we used co-activator binding profiles and genome topology measurements to predict the genes and CREs associated with transcriptional protein condensates. To accomplish this goal, we built BOUQUET, a computational pipeline that leverages a label-propagation machine learning method from graph theory to uncover the regulatory networks of transcriptional co-activator–bound CREs, or "communities". We find that, in single cells, genes within the same community have elevated degrees of co-expression, and CREs within the same community have correlated accessibility, consistent with these elements occupying a shared sub-nuclear environment. We observe that, in mESCs, the distributions of loading for Mediator subunits, BRD4, and other transcriptional proteins are asymmetric across communities and their summed levels significantly correlate with gene expression. Community composition reliably predicts the transcriptional impact following a variety of perturbations, including the deletion of constituent CREs and the depletion of a co-activator. We identify a subset of communities with exceptional co-activator signal and call them "3D super-enhancers", or "3D-SEs." 3D-SEs are enriched for genes that control specific cell identities across a variety of cell types. Extremely high-signal CRE assemblies, such as those at the histone-encoding gene loci that form the histone locus body condensate, are also 3D-SEs, despite being undervalued by current approaches. Finally, we confirm via fluorescence microscopy that *Sptlc2*, which shares a 3D-SE with the cell identity gene *Esrrb*, also shares its co-activator condensate; these genes are co-regulated, despite their sizable genomic separation. Together, our approach sheds light on the genes that

associate with spatial concentrations of co-activators and the genetic elements that regulate them, opening new lines of investigation into the functions of transcriptional condensates.

MATERIALS AND METHODS

Building Optimized Units of QUantified Enhancer Topologies (BOUQUET): inferring structure-informed gene regulatory communities

We built enhancer/promoter networks in mESCs by combining a reference gene list, an active enhancer map, an active promoter map, H3K27ac HiChIP loops, Insulated Neighborhoods (INs), and, optionally, topologically associating domains (TADs) (40).

Step 1: Building network of CREs: Nodes of the network, i.e. CREs, were defined using H3K27ac ChIP-seq and a reference gene annotation. Specifically, CRE nodes were the collapsed union of ChIP-seq-defined peaks and active gene promoters as defined in the Supplemental Methods. 11,051 collapsed regions that overlapped a promoter by >=1 bp were identified as promoter nodes, and H3K27ac ChIP-seq peaks that did not overlap at all were considered enhancer nodes. We added an edge between two nodes if they fit either or both of two criteria: 1) both nodes overlapped with the two anchors of the same HiChIP loop, defined above; 2) an enhancer node and a promoter node were both fully contained within the smallest IN, i.e. minimal number of bps, that contained the promoter (Supp. Data S1-S4).

Step 2: Identifying communities of CREs: With the CRE network as input, we employed the R package igraph (v.1.2.6) (41) to infer communities. Communities are defined in graph theory as sets of nodes that are highly interconnected, i.e., many edges connect nodes within a community, and few edges connect nodes from distinct communities (42). We used a modified Label Propagation (LP) algorithm with back-filling to detect communities of CREs for each expressed gene (43). We first identified subsets of nodes in the genome-wide network that are completely disconnected from others, i.e., network components. For a given gene within a component, the gene node and its neighbors, i.e., the CREs connected to it directly by loops or by INs, was initialized with the same community label whereas every other node in the component was initialized with a unique community label. At every

iteration of propagation, each node updates its community label to the one that occurs with the highest frequency among its directly connected neighbors. The LP algorithm resolves when every node within a component has the label that the maximum number of its neighbors also have. As labels propagate through the component, a single label can quickly become dominant in a densely connected group of nodes but will have trouble crossing a sparsely connected region of the component. As a result, densely connected groups of nodes quickly reach a consensus on a unique label. At resolution those nodes that are assigned the same label of the given gene are considered part of that gene's community. We appended a step to this established LP approach to ensure that directly linked nodes were captured; we used a back-filling method to rescue any directly linked nodes, i.e. CREs that loop to the promoter or that are within the same smallest IN as the promoter, that did not share the same community label of the given gene after LP process. Consistent with the graph theory literature, we refer to the highly interconnected subsets of nodes produced by this method as "communities" (Supp. Data S5).

Step 3: Calling 3D-SEs: We extracted 3D-SEs from all communities according to their constituent CREs' collective transcriptional protein coverage, which was calculated separately for each mark we studied, including co-activators, H3K27ac, CTCF, RONIN, etc. For each community and for each mark, we summed the relevant ChIP-seq reads across all its constituent CREs as its measurement of regulatory signal loading. When ranking communities by their regulatory signal loading, we observed a distribution where a limited number of communities have exceptionally high cumulative signal. We identified the point in the distribution at which the line y=x is tangent to the curve and used this point as a cutoff as described previously (13). Communities above this signal cutoff were defined as 3D-SE CRE communities (3D-SEs) (Supp. Data S6).

Step 4: Optional step for expanded CRE community assignment: Some researchers may be interested in studying the regulatory communities of CREs that are not covered by direct loops or by INs. If the optional "expanded CRE community assignment" feature is used, following the completion of the community detection process described above, any remaining unassigned, active enhancers that are within a TAD are assigned using a combined linear proximity/TAD approach. That is, the linearly most proximal promoters in both the upstream and downstream directions are considered for each enhancer, and the enhancer is

assigned to the most linearly proximal promoter within the same TAD, if any such promoter exists, using bedtools closest. TADs can constrain CRE interactions, potentially improving the accuracy of the linear proximity-focused, one-to-one assignment of enhancers to genes. We include this step as an opt-in assignment feature to facilitate near complete level of CRE community assignment, but it has lower precision than loop/IN-informed CRE connections (Supp. Fig. 1A) (40, 44–47).

BOUQUET-lite

Though its most obvious use case is assessing genome looping, H3K27ac HiChIP data implicitly measures proxies of additional gene regulatory properties, including CRE activity and gene expression. Thus, we believed H3K27ac HiChIP alone could be used to enable CRE community detection. We designed a version of BOUQUET, BOUQUET-lite, that uses only H3K27ac HiChIP, which enabled us to study CRE communities in additional mouse tissues where only H3K27ac HiChIP data were readily available. In case an enhancer map is not available in the matched cell type, an alternative method is available to infer candidate loop anchors using H3K27ac HiChIP itself. We used HiChIP-Peaks (v0.1.2) with "-f 0.4" to call enriched peak regions from H3K27ac HiChIP datasets and used the resulting peak set as active CREs. In parallel, promoters (TSS +/- 2kb) were ranked by their coverage of H3K27ac HiChIP reads calculated using bedtools intersect, and the top two-thirds were retained to represent expressed genes. H3K27ac HiChIP peaks and expressed promoters identified thusly were collapsed using bedtools merge to generate a set of candidate loop anchors, which were used as input for Hi-LOW as above. In case INs are not available, we relied strictly on H3K27ac HiChIP loops to infer CRE connections and build the initial network of CREs genome-wide (Supp. Data S7-S9). Finally, H3K27ac HiChIP read coverage was used to rank each community instead of co-factor ChIP signal.

These resulting loops, H3K27ac HiChIP peaks, and H3K27ac HiChIP coverage BAMs were used as input for BOUQUET-lite in the following cell/tissue types: mouse embryonic stem cells (GSE99519), thymocytes (GSM5268039), SST-neurons (GSM4551965), regulatory T cells (Treg) (GSM3059349), and cardiomyocytes (GSM6916796) (Supp. Data S10-S14). A cutoff for 3D-SEs was similarly defined as described above (Supp. Data S15).

CRE accessibility correlation – LASER

To calculate CRE accessibility correlation, we created a customized CRE-by-cell matrix. We quantified the accessibility of each CRE in each cell using the function FeatureMatrix() of the Signac package, using the fragment file and the CRE node list defined above as input. CRE read counts were normalized by the 'LogNormalize' method using the function NormalizeData().

To measure the correlation of pairwise CRE accessibility, we binarized (set CRE read counts to 0 or 1) the CRE-by-cell matrix and calculated the Odds Ratio (OR) using the 2 x 2 read count table for each pair of CREs. To test the statistical significance of CRE ORs between different groups, we used a bootstrapping technique to generate simulated CRE-by-cell matrices. This was done by randomly resampling cells with replacement, and it allowed us to compute the following statistic from each simulated matrix: the difference of median ORs between two groups, e.g., community vs. background. Since this statistic largely follows a binomial distribution (with only 29 out of 570 bootstrap distributions showing significant p-values (<0.05) by the Shapiro-Wilk test across bootstrap simulations), we calculated a p-value while assuming the null hypotheses, i.e. that there is no difference of OR between the two groups compared. We developed a method, Loci ATAC-Seq Enrichment Resampling (LASER), to perform the process described above. The LASER method is estimated to run in time $O(n^2)$ (with n being the number of total CREs), making the method computationally intractable for calculating all genome wide CRE pairs at once. To overcome this limitation, LASER splits the genome into pairs of chromosomes (190 pairs of 20 mouse chromosomes) and calculated correlations between peaks on all pairs of chromosomes in parallel. This method substantially reduced runtime and made it feasible to calculate pairwise CRE accessibility correlation genome wide.

See Supplementary Material for detailed materials and methods.

RESULTS

Assembling CRE communities using BOUQUET

We developed "BOUQUET" (Building Optimized Units of QUantified Enhancer Topologies), a computational pipeline that uncovers communities of co-activator–bound CREs based on genome-wide CRE interactions (Fig. 1A, Supp. Fig. 1A, Methods) (17, 31). Our fundamental hypothesis is that accurate assignment of transcription apparatus using genome organization will aid the identification of collections of especially-protein-rich genome regions that are associated with nuclear condensates. To accomplish this goal, BOUQUET connects CREs into networks using high-confidence topology measurements, uses a label-propagation machine learning algorithm from graph theory to subdivide CRE networks into highly interconnected sets called "communities," and quantifies these communities based on their summed transcription protein signal at their constituent CREs (Methods, Supp. Data S1-S5). BOUQUET begins by considering a pair of CREs to be connected if they meet at least one of two criteria: they are connected by a high-confidence HiChIP loop; or they are contained within the same Insulated Neighborhood (IN) (see Methods). Insulated Neighborhoods (INs) are chromatin loops formed by contacts between CTCF/cohesin-bound regions whose disruption can impact the regulation of transcriptional bursting by chromatin condensates (9, 35–37). Our use of IN-derived connections is supported by the similar read counts observed for CRE-pairs connected by high-confidence loops versus CRE-pairs connected by INs but not high-confidence loops when such CRE-pairs are separated by similar distances (Supp. Fig. 1B) (48). Using only high-confidence HiChIP loops in mouse embryonic stem cells (mESCs), only 74.8% of the active enhancers and 81.3% of the active promoters in mESCs were directly connected to another activating CRE; further, not every high-confidence loop connected pairs of activating CREs (Supp. Fig. 1C, D). When we combined high-confidence H3K27ac HiChIP loops and INs, we could link 89.9% of active enhancers and 91.9% of active promoters to at least one other CRE, giving us a near-comprehensive coverage of activating CREs by genome topology (Supp. Fig. 1C).

We applied BOUQUET to identify CRE communities in mESCs, a well-established system for the study of co-activator condensates and their associated genes (4–7). For 23,084 active genes in mESCs, we identified 11,051 communities, with a median of 7 CREs per community. There was an overall positive correlation (Spearman rho = 0.46, p-value = 1.6×10^{-245}) between the numbers of promoters and enhancers within a community, but a few showed a

bias toward either promoters or enhancers (Supp. Fig. 1E). We next quantified ChIP-seq of MED1 at communities as an initial representative co-activator because of its established association with large CRE collections and transcriptional condensates, its mechanistic role in the facilitation of physical connectivity of TF-bound enhancers to promoters, and its regulation of Pol II elongation (49). Several properties of CRE communities are highly correlated, e.g., communities with greater numbers of CREs tended to also have higher MED1 signal, greater numbers of overall interactions (i.e. "edges"), and greater number of interactions from the community's focal gene (Supp. Fig. 1F, Methods) (16).

Elements of the same community show elevated activity correlation

Having identified CRE communities genome-wide, we next investigated the properties of CREs assigned to the same community. If the CREs within communities are functionally linked by sharing the same sub-nuclear environment, we would expect that elements of the same community would demonstrate higher levels of coordination in their activities, i.e. gene expression and CRE activity. To test this hypothesis, we generated scRNA-seq in mESCs. Though clusters were algorithmically identified, the whole sample showed overall homogeneity in expression profiles, which supported our use of each cell as a replicate (Fig. 1B). For each pair of expressed genes (gene-pair), we calculated Spearman's correlation coefficients for their expression levels across all cells (Fig. 1C). For gene-pairs that were not part of the same community, the median expression correlation level was low (r=0.0065). In contrast, gene-pairs within the same community showed a two-fold higher median expression correlation level (r=0.02) and a significant but modestly higher trend of co-expression than non-community gene-pairs ($p = 2.23x10^{-308}$, two-sided Wilcoxon Rank Sum Test). The statistically significant correlation between shared community membership and gene co-expression held across eight other commonly used statistical tests of correlation (Supp. Fig. 1G). This finding supports the hypothesis that gene expression is more tightly coordinated among genes that share a community than between genes that do not, but this correlation is modest, likely due to the complex set of processes that contribute to expression.

To further examine the degree of coordinated CRE activity within communities, we performed single-cell ATAC-seq (scATAC-seq) in mESCs. ATAC-seq measures chromatin accessibility to the Tn5 transposase, which is an indicator of a region's ability to bind to transcription-regulating proteins that may be used as a proxy for enhancer activity (50–52). UMAP clustering analysis of our scATAC-seq data reiterated that our cell population is generally homogeneous, here at the chromatin accessibility level, supporting our handling of cells as replicates (Fig. 1D). In contrast to scRNA-seq, there is an upper limit on the number of ATAC-seq integration sites across two copies of the same CRE, which compresses the possible dynamic range of measurements at a given locus (50). To perform robust statistical analyses of co-accessibility, we developed an algorithm that overcomes this range limitation, Loci ATAC-Seq Enrichment Resampling or "LASER," which calculates odds-ratio-based measurements of the co-accessibility of CRE-pairs across a set of individual cells. We used LASER to establish a background CRE co-accessibility distribution against which to evaluate the co-accessibility of CREs within a single community by randomly selecting pairs of CREs not from the same community. We compared the co-accessibility of these randomized CRE-pairs with pairs of CREs within the same community (Fig. 1E). CRE-pairs within the same community showed a significant but modestly higher trend of co-accessibility than randomized non-community CRE-pairs (median Odds Ratio = 0.58 vs. 0.52, respectively; $p=1.6x10^{-25}$, bootstrapping procedure). Altogether, these results suggest that activities of within-community CREs are correlated, but these correlations are modest, likely due to the influences of additional gene regulatory processes.

BOUQUET communities recapture CRE sets that regulate condensate-associated genes

We next probed the communities of known co-activator condensate-associated genes for confirmed and novel CRE relationships. One such gene of interest is *Sox2*, which encodes a master transcription factor that regulates pluripotency and associates with condensates of BRD4 and of MED1 in mESCs. (9, 53–58). Previous studies revealed that *Sox2* is regulated by both a proximal linear SE and a distal SE approximately 100 kb downstream, called the "Sox2 Control Region" (SCR) (Supp. Fig. 2A) (13, 57, 59). Further, three-way microscopy imaging previously revealed the SCR's role in regulating transcriptional bursting of *Sox2* during interactions among *Sox2*, the SCR, and transcriptional condensates (9). Consistent with this

work, our pipeline highlighted interactions between *Sox2*'s promoter and both the proximal linear SE and the SCR, and that all of these elements were within the same CRE community (Supp. Fig. 2A, B). Further, BOUQUET's prediction that *Sox2* is the only protein-coding gene in its community was validated by the previous observation that genetic deletion of the SCR in mESCs only significantly impacts the expression of *Sox2*, leaving the expression of surrounding, linearly proximal genes unaffected (57). Consistent with the association of *Sox2*, the SCR, and co-activator condensates, *Sox2*'s community was in the top 1% most MED1-rich and top 2% most BRD4-rich (Supp. Data S5).

A second gene of interest is *D7Ertd143e*, a mammal-specific polycistronic pri-microRNA, whose mature miRNAs, *miR290* through *miR295*, regulate ESC pluripotency. *D7Ertd143e* has been shown to associate with nuclear co-activator condensates of MED1 and of BRD4 and, correspondingly, the largest linear SE (Supp. Fig. 2C) (4, 60). Previous single-gene expression analysis showed that deleting a CRE within the *D7Ertd143e*-associated SE caused significant downregulation of *D7Ertd143e*. BOUQUET confirmed that the deleted CRE and *D7Ertd143e* were indeed within the same community in wild-type cells. We performed RNA-seq on CRE-deleted cells to study the effects of CRE deletion on other genes within the *D7Ertd143e* community (Supp. Fig. 2C, D, E, Supp. Data S16, S17) (61). As expected, we observed significant downregulation of *D7Ertd143e* in CRE-deleted cells (p-value=2.77×10^{-107}) (61). Additionally, we found that the genes in the *D7Ertd143e* community were, on the whole, significantly more downregulated than control genes ($p=5.9 \times 10^{-4}$, Wilcoxon Rank Sum Test, two-sided) and that all but one expressed gene in the *D7Ertd143e* community were significantly downregulated (Supp. Fig. 2E, Supp. Data S17). Notably, expression was not diminished for genes immediately beyond the linear boundaries of the community, despite all of the community and linearly proximal genes being within the same TAD (Supp. Fig. 2E, Supp. Data S17). Consistent with the association of *D7Ertd143e*, its SE, and co-activator condensates, *Mir290'*s community is in the top 1% most MED1-rich or top 1% BRD4-rich (Supp. Data S5). These results suggest that large communities uncovered by our approach accurately predict the genes that will be affected by CRE perturbation.

Community co-activator signal correlates with gene expression and expression response to co-activator perturbation

Previous CRISPR tiling screens showed that the effect of perturbing a given CRE on its target gene correlates with that CRE's ChIP-seq signal (called "activity") and its frequency of contacting the target gene (62). We therefore hypothesized that target gene expression should directly correlate with CRE signal, but this relationship would only be revealed if all relevant CREs were accurately associated with their target genes and their signal were combined. To test this hypothesis, we compared gene expression against BOUQUET-assigned co-activator signal or against genomically proximal co-activator signal using ROSE. The combined MED1 signal at each CRE community was significantly correlated with the expression of genes within that community by bulk RNA-seq in mESCs (Spearman rho=0.27, p-value=1.3×10^{-198}) (Fig. 1F, Supp. Data S5). In contrast, genomically linear enhancer/co-activator assignment showed much lower and insignificant correlation to expression levels of their assigned target genes (Spearman rho=0.02, p-value 0.0665) (Fig. 1G, Supp. Fig. 2F, Supp. Data S18). These results suggest both that accurately assigned co-activator signal better correlates with expression level and that topology-informed BOUQUET communities more accurately capture the co-activator–bound CREs relevant to target gene regulation.

If co-activator signal within a community is predictive of gene expression, then loss of that co-activator might more dramatically affect high-signal communities. To test this hypothesis, we acquired RNA-seq data from mESCs after *Med1* had been knocked-down (63). As hypothesized, there was a significant negative correlation between the expression response to *Med1* knock-down and MED1 signal assigned to a gene by BOUQUET; genes downregulated most profoundly were among the most MED1-rich communities, and vice versa. (Spearman = -0.14, p-value = 1.26×10^{-50}) (Fig. 1H, Supp. Data S19). In contrast, expression response to *Med1* knock-down showed no correlation with co-activator signal assigned by genomic proximity (Spearman = 0.01, p-value = 0.448) (Fig. 1I, Supp. Data S19). Thus, protein signal associated with genes using genome topology quantitatively predicts expression and response to perturbation.

High correlation among activator marks at communities

Multiple transcriptional proteins form condensates and may be heterogeneously responsible for gene regulation by distinct CREs (4, 6–9, 64, 65). We therefore hypothesized that communities could be differentially enriched in different co-activators. We compared the genome-wide distributions of MED1, BRD4, CBP, or EP300 because each of these factors bind active CREs genome-wide, but they have distinct mechanisms of action. We confirmed that they have partially distinct binding sites across the genome but a high degree of correlation overall (Supp. Fig. 3A, B) (29). We also examined H3K27ac, a histone modification that marks nucleosomes adjacent to active CREs and that is commonly used for super-enhancer analysis (39, 66). The genome-wide distribution of H3K27ac was significantly correlated to that of the co-activators, making it an attractive alternative for studying systems where limited datasets are available (Supp. Fig. 3A, B). In contrast, other condensate-forming proteins (RONIN, CTCF) did not show similar degrees of correlation genome-wide (Supp. Fig. 3B) (6, 29, 67–69). The high correlation between activation marks was more pronounced when marks were compared using within-community signal (Supp. Fig. 3C, Supp. Data S5). Again, CTCF and RONIN did not show similar degrees of correlation at BOUQUET-derived communities, which we interpret to be due to their distinct preference for genomic regions (insulators and certain activating CREs for CTCF, housekeeping gene promoters for RONIN) (Supp. Fig. 3C, Supp. Data S5) (6, 29, 67, 68). Thus, despite some variation in each factor's mechanism of action and chromatin binding at the individual-CRE level, co-activators are generally correlated in their collective accumulation at CRE communities.

Similar to MED1, we found that communities with higher accumulated levels of activation marks contained genes with higher levels of community gene expression (Fig. 2A). As seen for MED1, this correlation was stronger than the correlation of gene expression with linear-genome-based assignment of signal for the same factors (Supp. Fig. 3D, Supp. Data S20-S23). Thus, community signal for all tested activation marks correlates highly with community gene expression.

3D-super-enhancers

A thorough literature review uncovered that, in mESCs, condensates of specific co-activators have been shown to interact with 7 genes, all of which control cell identity, and whose associated chromatin sites are associated with SEs highly enriched for co-activator binding: *Esrrb* (MED1), *Nanog* (MED1, BRD4), *Mir290* (MED1, BRD4), *Sox2* (BRD4), *Trim28* (MED1, BRD4), *Klf4* (MED1, BRD4), and *Pou5f1* (BRD4) (4, 6, 7, 10, 70). We therefore hypothesized that the genes within CRE communities that had exceptionally high co-activator signal may be enriched for cell-identity-defining genes (4–6, 9). We began by ranking communities by their signal enrichment for MED1, BRD4, EP300, CBP, and H3K27ac. We observed an asymmetric distribution of cumulative protein signal across communities for each mark; in each case, most communities accumulated a modest amount of signal, whereas a minority of communities (<10%) accumulated an exceptional amount of signal (Fig. 2B).

Irrespective of the mark used to stratify communities, we noted qualitative similarities between how co-activator signal was distributed across communities and well-established co-activator signal distributions at CRE clusters assembled by genomic proximity (13, 14, 39). Exceptionally high-signal linear CRE clusters have been studied in great detail as "super-enhancers;" as an evolution of this concept, we chose to term the exceptionally high-co-activator subset of our topology-based CRE communities "3D super-enhancers", or 3D-SEs (Supp. Data S6). To define this subset mathematically, we used the established signal cutoff strategy from the linear SE software, ROSE (Methods) (13, 14, 39). All but one known co-activator condensate-associated genes were in 3D-SEs defined by all analyzed co-activators; the lone exception was *Trim28*, which was associated with MED1-ranked, BRD4-ranked, and H3K27ac-ranked 3D-SEs but was sub-threshold when communities were ranked by EP300 and CBP (Fig. 2B). Intriguingly, the numbers of 3D-SEs for MED1 and BRD4 (1,158 and 986) more closely comport with the number of observed MED1 and BRD4 protein foci in mESC immunofluorescence (~1,000) than the number of MED1 or BRD4 linear SEs (214 and 422), which suggests that 3D-SEs might correspond more comprehensively to co-activator condensates (Supp Data S18, S20) (4).

3D-SEs had a greater degree of factor-specificity than moderate-signal communities (Fig. 2C). An analysis of the coefficient of variance for 3D-SEs using their relative enrichment in MED1, BRD4, EP300, and CBP showed that a subset of communities was relatively rich in certain co-activators and relatively poor in others (Supp. Fig. 3E, F, Supp. Data S24,

Supplemental Methods). This observation suggests that not all genes that are associated with one type of condensate might be expected to be associated with other types of condensate.

Though both were derived by identifying signal-rich CRE collections, we noted interesting differences between linear SEs and 3D-SEs (Supp. Fig 4A). For example, the histone gene clusters are predominantly regulated by promoter elements and are also known to form the biomolecular condensates known as the "Histone Locus Bodies" (71). However, despite their enrichment for marks of activating chromatin, these gene clusters have not been associated with linear SEs (Supp. Fig. 4B, C) (71). Consistent with its apparent chromatin signal, *H2ac10*, a representative gene from this cluster and one of 23 total histone genes associated with MED1 3D-SEs, is associated with 3D-SEs defined by all analyzed factors (Fig 2C). Thus, the strategy underpinning BOUQUET enables assignment of high signal to condensate-associated genes with distinct CRE network properties.

We performed a gene ontology analysis of the genes associated with MED1 3D-SEs. As anticipated, the most significantly enriched term was "Embryonic Stem Cells." (Fig 2D, Supp. Data S25). We next compared MED1-identified 3D-SEs with those identified by BRD4, EP300, CBP, or H3K27ac. We found that the most significantly enriched term was consistently "Embryonic Stem Cells" (Fig. 2D, Supp. Data S25). Indeed, there was a significant genome-wide correlation between community signal loading and ESC-relevant genes via pre-ranked Gene Set Enrichment Analysis (Fig. 2E, Supp. Data S26). Thus, 3D-SEs comprise CREs and target genes that assemble large amounts of specific co-activator apparatus and are associated with cell-identity-defining genes and other extremely highly regulated genes.

3D-SEs are enriched in cell identity genes across mammalian tissues

We next sought to determine whether 3D-SEs were specific to ESCs or could be found in other mammalian tissues. To enable community identification across a broad range of systems, we designed BOUQUET to be compatible with a variety of input datatypes. For use in tissues and cells where the preferred datasets may be unavailable, we implemented a minimal protocol (BOUQUET-lite) that only requires H3K27ac HiChIP, which generally reflects

topological interactions, CRE activity, and gene expression, albeit with certain limits (Methods). The characteristics we observed in mESC "full" BOUQUET communities were generally consistent with communities derived from BOUQUET-lite. Specifically, both protocols uncovered comparably shaped distributions of signal across communities genome-wide, a high correlation between community signal and community gene expression, and recovery of known co-activator condensate-associated genes within 3D-SEs (Supp. Fig. 5A, 5B, Supp. Data S15). As such, we propose that BOUQUET-lite is an appropriate substitute for studying communities in systems with limited data.

To interrogate CRE communities in differentiated mammalian cell types, we executed BOUQUET-lite on published H3K27ac HiChIP datasets in mESCs and four other mouse cell/tissue types: cardiomyocytes, somatostatin (SST)-expressing neurons, thymocytes, and regulatory T cells (Treg) (Supp. Data S10-S14) (72–75). Consistent with our observations in full BOUQUET for mESCs, cumulative community H3K27ac signal was significantly positively correlated with community gene expression in all cell/tissue types (Fig. 3A). We noted asymmetric distributions of H3K27ac signal across communities genome-wide, with small fractions of communities that were exceptionally signal-rich in each cell/tissue type (Fig. 3B). Altogether, these results demonstrate that co-activator–rich CRE communities are a general phenomenon found across tissue types.

We next examined the genes associated with CRE communities and their specificity across cell types. Genes associated with 3D-SEs tended to be associated with 3D-SEs in only one cell type, whereas genes in moderate-signal communities were largely shared across multiple cell/tissue types (Fig. 3C, Supp. Data S15). Though certain genes were in 3D-SEs in multiple cell types, including several groupings of histone genes, we observed variability in the structures of those 3D-SEs (Fig. 3B, Supp. Fig. 6A-C, Supp. Data S15). This observation suggests that genes are generally associated with 3D-SEs in a cell-type-specific manner and that, when associated with 3D-SEs in multiple cell types, their CRE composition can also be cell-type-specific.

If genes are associated with 3D-SEs in a cell-type-specific manner, it would be expected that these genes have roles in executing or establishing those cell identities. We performed gene ontology analyses in each cell/tissue type to determine whether 3D-SE-associated genes are

enriched for genes associated with identity-defining functions across the body (Fig. 3D, Supp. Data S25) (4–7, 9). Genes associated with 3D-SEs were indeed specifically enriched for signature factors known to contribute to specialized cell identities and functions, consistent with their source cell/tissue type, e.g., *Pml* in mESC, *Actn2* in cardiomyocytes, *Nxph1* in SST-neurons, *Cd8a* in thymocytes, and *Itk* in Treg cells (Fig. 3B, Supp. Fig. 7A, 7B) (76–80). Further, the composition of these 3D-SEs, including both constituent CREs and the connections among them, were cell-type-specific. Pre-ranked Gene Set Enrichment Analysis showed that, in a given cell type, elevated community signal was significantly linked to roles in cell identity (Supp. Data S26) (Fig. 3E). Together, these results suggest that the regulatory communities associated with high levels of transcriptional machinery are specifically enriched for cell identity genes across mammalian tissues.

3D-SEs inform expression responses to signaling pathways

The heterogenous binding of TFs at CREs has been proposed as a mechanism by which a variety of cellular signals can be integrated into a gene's expression, especially for key cell identity genes associated with multiple CREs (61). Moreover, co-activator condensates have been observed to sequester high concentrations of signaling transcription factors (sTFs) (70). We thus hypothesized that 3D-SEs integrate cellular signals and enable elevated community-spanning responses to multiple signaling pathways. To test this hypothesis, we reanalyzed ChIP-seq data from three terminal TFs of notable signaling pathways relevant in mESCs: STAT3, SMAD3, and TCF3 (81–83). We examined the CREs of 3D-SEs, moderate-MED1-signal communities, and size-matched randomized control sets of CREs, to determine whether each set of CREs was collectively bound by 0, 1, 2, or 3 types of signaling TFs (Supplemental Methods; Supp. Fig. 8A). Most 3D-SEs (60%) contained binding events for all three types of sTF, which was significantly more than moderate-MED1-signal CRE communities (8%) or randomized communities of the same size (39%, two-sided Chi-squared test P-value=1.5×10^{-49}). Further, 3D-SE genes showed a greater change in gene expression following signaling pathway perturbation: TGF-β pathway perturbation (suppressing expression by blocking Tgf-β with SB431542; $p = 2.9 \times 10^{-15}$), LIF pathway stimulation (activating expression by exposing to LIF for 1h; $p = 3.9 \times 10^{-7}$), and Wnt pathway perturbation (activating expression by *Tcf3*

knockdown; $p=5.4 \times 10^{-9}$) (Supp. Fig. 8B, Supp. Data S27). Interestingly, 3D-SE genes were more dramatically responsive to signaling perturbation than the genes that were the nearest linear neighbors of signaling-TF-bound CREs (Supp. Fig. 8C). Altogether these results demonstrate that 3D-SEs amplify the gene expression responses to critical transcriptional signaling pathways by accumulating heterogeneous CREs.

3D-SEs as transcriptional condensate components

Several transcriptional proteins, including MED1 and BRD4, form high-density condensates that are observable in fluorescence microscopy experiments as punctate nuclear signals within a dilute background (2, 4, 6, 7). Based on their exceptional protein concentrations, we hypothesized that the CREs of 3D-SEs would interact with co-activator puncta, thus establishing BOUQUET as a genome-wide identifier of condensate-associated genomic regions. To test this hypothesis, we used fluorescence microscopy to study the largest 3D-SE in mESCs, ranked 1st by MED1 signal, and 3rd by BRD4 signal (Fig. 4A). This community comprises three Insulated Neighborhoods that each contain at least one signature protein-coding gene, *Esrrb*, *Irf2bpl,* and *Sptlc2*, so we refer to it as the EIS community. The EIS community spans ~1MB, which minimizes the likelihood that co-localization observations between elements at its most extreme ends would arise from stochastic chromatin movements. The EIS community locus is therefore ideal to study the interactions and activities of a broad, protein-rich community.

All genes that have been observed to interact with co-activator condensates had been previously assigned to linear super-enhancers, e.g., *Esrrb* from the EIS community. However, the closest linear super-enhancer to *Sptlc2* is over 400 kb away, and it is instead assigned to *Irf2bpl* (Supp. Data S18). To determine if the high community signal associated with *Sptlc2* by BOUQUET accurately predicted the interactions of *Sptlc2* with co-activator condensates, we performed DNA FISH and anti-BRD4 immunofluorescence in >100 mESCs (Fig. 4B, Supp. Fig. 9A). We searched 0.4 μm regions of interest (ROIs) centered on *Sptlc2* gene signal and found 12.6% (25 out of 199) indeed co-localized in this small region with punctate BRD4 co-activator signal (Fig. 4C). Unlike *Sptlc2*, *Esrrb* has been assigned a linear SE, which is intragenic to *Esrrb* (Supp. Data S18). As a comparison, the frequency of co-localization between *Esrrb* and BRD4 puncta was modest (2.3%, 5/219) (Supp. Fig. 9B), despite previous

deep study of the interactions between *Esrrb* and co-activator puncta (6). Thus, BOUQUET can identify 3D-SEs that predict the interaction of unexpected genes with co-activator condensates.

Since *Esrrb* and *Sptlc2* are within the same 3D-SE and have been shown to interact with co-activator puncta, we hypothesized that both genes could interact with the same individual punctum (4, 6). 0.4 μm ROIs were constructed around *Sptlc2* or *Esrrb* DNA FISH puncta, and we characterized their co-localization as well as their tripartite interactions with BRD4 puncta. The genes that encode *Esrrb* and *Sptlc2* frequently co-localized in these small regions, and several of these co-localized occurrences also overlapped BRD4 foci (Fig. 4C, Supp. Fig. 9B). These results suggest that both genes are simultaneously interacting within the same individual punctum instead of with distinct co-activator puncta.

Using higher-resolution experiments, we next examined how co-localization of genes related to coordinated transcriptional regulation. Single-cell RNA-seq demonstrated that most cells contained transcripts of both *Esrrb* and *Sptlc2* (77%) (Supp. Fig. 9C), and single-cell ATAC-seq demonstrated that both of their promoters were transposase-accessible (64%) in the vast majority of cells (Supp. Fig. 9D). However, these assays do not directly interrogate the coordination of gene transcription or CRE activity, nor how this coordination relates to co-activator signal. To measure coordinated transcription, we designed RNA FISH probes to mark only the nascently transcribed RNAs of *Esrrb* and *Sptlc2* and studied their expression patterns in mESCs bearing endogenously tagged meGFP-MED1 (Fig. 4D, Supp. Fig. 9E, Supplemental Methods). These RNA probes therefore also mark the precise nuclear region containing the gene being transcribed.

We defined 357 regions of interest (ROIs) as 0.4 μm nuclear regions that contained a punctum for at least one nascent transcript. Most co-activator puncta and their associations with genes are short-lived, and RNA transcription is infrequent and bursty, complicating analysis of their coincidence (6, 9, 84). To establish a background expectation, we examined the 145 ROIs that were positive for *Esrrb* transcription and observed that only 3.4% of such ROIs coincided with punctate MED1 signal (Supp. Fig. 9F). We observed a comparable fraction, 2.2% of 229 ROIs with *Sptlc2* transcription, coincided with punctate MED1 signal.

Thus, *Sptlc2* interacts with co-activator puncta with comparable frequency as *Esrrb* whose interactions with co-activator puncta have been detailed.

We next examined the relationship between co-transcription and co-activator puncta. As expected, only 4.8% of 357 ROIs contained both *Esrrb* and *Sptlc2* transcription. Consistent with the observation that *Esrrb* and *Sptlc2* DNA are likely to interact within the same BRD4 punctum, we see that in ROIs with co-transcription, 18% (3/17) showed RNA co-localization with MED1 puncta. We repeated this experiment with cells bearing BRD4-meGFP and also observed three-way co-localization between nascent *Esrrb* RNA, nascent *Sptlc2* RNA, and BRD4 puncta in these cells (Supp. Fig. 9G). Thus, 3D-SEs contain genes that are co-transcribed and co-localize with the same co-activator punctum. Altogether, via genome-wide unbiased analysis, BOUQUET identifies genes that interact with co-activator puncta at similar frequency as genes previously studied in great detail for their interactivity with such puncta.

DISCUSSION

Understanding which cis-regulatory elements (CREs) and associated transcriptional machinery regulate each gene is critical to decoding gene regulation and cell identity. Popularly used methods for unbiased CRE-gene assignment are limited in their ability to incorporate chromatin topology; as a result, these approaches can neither capture the full complexity of CRE function nor fully account for the transcriptional apparatus relevant for a given gene's regulation. Attempts to predict the regulatory contributions of given CREs by combining individual CRE activity and their direct genomic contacts have uncovered several quantitative relationships that connect chromatin measurements to expression, but these approaches ultimately do not interrogate the known multi-faceted interactions of multiple enhancers with multiple promoters observed in mammalian cells. A more comprehensive approach would capture the entire set of regulatory elements that impact a given gene's expression. This philosophy has guided other groups to develop models of transcriptional "hubs" or "highly interconnected enhancers" that represent individual CREs with many interaction partners (16, 17, 38). While the hub model can identify sets of CREs associated with a single focal node using direct loop connections, it can lack broader context of how

genes and CREs throughout that same region interact with each other in interconnected networks. Further, these approaches are ultimately limited by statistical challenges in setting appropriate significance thresholds for loop-identification, since they exclude connections that are sub-threshold. The limitations of these approaches inspired us to develop a strategy to optimally assemble CREs and associated protein apparatus.

Recent studies have revealed that collections of co-activator protein within the nucleus often are associated with liquid-liquid phase-separated (LLPS) droplets or transcriptional condensates; additional physical models and terms have been proposed and are under ongoing study. Irrespective of biophysical process, being able to predict which genes and regulatory elements may functionally associate with these protein foci is of prime interest. The field is limited in its studies because fewer than 10 genes have been observed to associate with co-activator condensates, but more than a thousand co-activator foci have been observed per nucleus. Other chromatin proteins that form condensates may have similar discrepancies. Here, we describe BOUQUET, a novel computational framework that quantifies the transcriptional protein apparatus associated with a given gene by detecting the gene's regulatory community via well-characterized categories of topological interaction. To our surprise, we uncovered a significant correlation between the amount of protein apparatus we could assign to a gene's community and that gene's expression; this relationship is intuitive but (to our knowledge) has not been reported, which we suppose is due to long-standing difficulties with CRE-gene assignment. The uneven or asymmetric distribution of proteins at communities enabled us to identify an extremely protein-rich subset of communities we refer to as "3D-super-enhancers." 3D-SE genes include all known condensate-associated genes, and the number of 3D-SEs roughly matches the number of condensates. We demonstrate that at least one gene not previously associated with a linear SE is condensate-associated, suggesting that 3D-SEs might correspond to co-activator condensates.

Unsurprisingly, many of our 3D-SE genes included many of the same cell-identity-defining genes previously identified as associated with linear SEs; however, through the inclusion of topology, we can more expansively characterize the gene regulatory interactions associated with those genes and nominate additional CREs putatively involved in regulating their expression. It is likely that each CRE within a community contributes to the regulation of each

gene within that same community in a distinct manner, including the possibility of redundancy, additivity, synergy, competition, and/or hierarchy among community CREs, especially as they respond to distinct sets of signaling pathways (74, 85). Here, we proposed additivity of signal among activating CREs would be a reasonable measure of community activity, but other strategies to combine CREs of different types and their associated signal may refine our findings. We are also able to identify high-signal communities overlooked by enhancer-biased alternatives, such as the promoter-heavy condensate-forming histone gene cluster (71). Based on our findings, it also seems likely that multiple SE-associated genes can be co-regulated within the context of a single community, such as the *Esrrb-Irf2bpl-Sptcl2* 3D-SE community (Supp. Data S18). This finding suggests that the study of mutant enhancers should similarly expand if topology is considered and should improve the prediction of the effects of non-coding mutation.

It has been observed that co-localized genes are co-expressed and that co-localized enhancers are coordinately active (86, 87). Our CRE communities provide an effective framework for identifying CREs whose regulatory activities are linked. Indeed, we observed a colocalization between co-activator puncta and multiple components of the largest 3D-SE (containing *Esrrb; Irf2bpl; Sptlc2;* et al.*)* when multiple constituent genes were both expressed and in proximity. These observations demonstrate that 3D-SEs can be observed in single cells, are not merely an artifact introduced by HiC technologies, and that multiple genes can be arranged near or in the same co-activator punctum. Our microscopy data suggest that CREs collaborate to regulate gene expression within a 3D-SE through multi-partite physical interactions. Several technical challenges limit our assessment of co-localization with immunofluorescent imaging, including probe intensity, photobleaching, relocation misalignment, and the stringency of our analysis using sub-micron regions of interest. We therefore believe our evaluations underestimate the close and frequent spatial arrangements of co-activator puncta and CRE communities. Further, transcriptionally productive associations between condensates and their gene targets have been shown to be highly transient (~12 seconds), increasing the likelihood that co-localization events may be too brief to be captured by static imaging approaches (6). Nonetheless, the findings of this study provide a valuable direct comparison of the co-localization of nucleic acids as measured by two commonly used orthogonal approaches, microscopy and sequencing-based

chromosome conformation capture. Future efforts will be needed to disentangle the roles of different CREs and regulatory proteins in governing gene expression within these complex networks, as well as the kinetics and frequency of each event, including punctum lifecycles. Ultimately, by accounting for the various layers of physical arrangement of the nucleus—chromatin composition, genome structure, and condensate assembly—when tallying the transcriptional apparatus that is relevant to the regulation of each gene, we can more accurately reflect biological reality and offer new insight into the fundamentals of gene regulation.

ACKNOWLEDGEMENTS

We thank Richard A. Young (Whitehead Institute) for providing parental mESC V6.5 and deletion (dMir290e) mESC V6.5 lines. We thank Charles H. Li, Abraham S. Weintraub, and Tong Ihn Lee for early conceptual discussions. We thank Sarah August for the editing support.

AUTHOR CONTRIBUTIONS

Jie Lv: Conceptualization, Data Curation, Formal Analysis, Investigation, Methodology, Software, Visualization, Writing – Original Draft. Kelsey A. Maher: Data Curation, Formal Analysis, Investigation, Software, Visualization, Writing – Original Draft. Li Dong: Investigation. Virginia Valentine: Investigation. Alaguraj Veluchamy: Data Curation, Formal Analysis, Software. Tilley Tian: Investigation. Yuna Kim: Investigation. Bensheng Ju: Investigation. Marc Valentine: Resources, Visualization. John Easton: Resources. Steven Burden: Formal Analysis, Investigation, Resources, Visualization. Stanley B. Pounds: Formal Analysis, Methodology, Resources, Software, Visualization. Brian J. Abraham: Conceptualization, Formal Analysis, Funding Acquisition, Methodology, Software, Supervision, Visualization, Writing – Original Draft.

SUPPLEMENTARY DATA

Supplementary Data are available at NAR online.

CONFLICT OF INTEREST

BJA is a shareholder in Syros Pharmaceuticals, which has licensed intellectual property regarding super-enhancers. All other authors declare they have no competing interests.

FUNDING

This work is supported by the Transcription Collaborative of St. Jude Children's Research Hospital [to B.J.A.]; and the American Lebanese Syrian Associated Charities (ALSAC) [to B.J.A.].

DATA AVAILABILITY

Data generated in this study have been deposited to the Gene Expression Omnibus (GEO) under accession number GSE254728. Publicly available datasets used in this study are detailed in Supplemental Data S28. UCSC Genome Browser tracks can be viewed at: https://genome.ucsc.edu/s/abraham_lab/3DSE_mm10. Code generated in this study is available at the following Github repositories: Hi-LOW (https://github.com/stjude/HiLOW; 10.5281/zenodo.15786041); BOUQUET (https://github.com/stjude/BOUQUET/; 10.5281/zenodo.15782836); LASER (https://github.com/stjude/LASER; 10.5281/zenodo.15786043); Insulated Neighborhood Caller (https://github.com/stjude/Dowen_Fan; 10.5281/zenodo.15784157).

REFERENCES

1. Hnisz,D., Shrinivas,K., Young,R.A., Chakraborty,A.K. and Sharp,P.A. (2017) A Phase Separation Model for Transcriptional Control. *Cell*, **169**, 13–23.

2. Niu,X., Zhang,L., Wu,Y., Zong,Z., *et al.* (2023) Biomolecular condensates: Formation mechanisms, biological functions, and therapeutic targets. *MedComm (Beijing)*, **4**, e223.

3. Demmerle,J., Hao,S. and Cai,D. (2023) Transcriptional condensates and phase separation: condensing information across scales and mechanisms. *Nucleus*, **14**, 2213551.

4. Sabari,B.R., Dall'Agnese,A., Boija,A., Klein,I.A., *et al.* (2018) Coactivator condensation at super-enhancers links phase separation and gene control. *Science*, **361**.

5. Boija,A., Klein,I.A., Sabari,B.R., Dall'Agnese,A., *et al.* (2018) Transcription Factors Activate Genes through the Phase-Separation Capacity of Their Activation Domains. *Cell*, **175**, 1842-1855.e16.

6. Cho,W.-K., Spille,J.-H., Hecht,M., Lee,C., *et al.* (2018) Mediator and RNA polymerase II clusters associate in transcription-dependent condensates. *Science (1979)*, **361**, 412–415.

7. Li,J., Hsu,A., Hua,Y., Wang,G., *et al.* (2020) Single-gene imaging links genome topology, promoter–enhancer communication and transcription control. *Nat Struct Mol Biol*, **27**, 1032–1040.

8. Ma,L., Gao,Z., Wu,J., Zhong,B., *et al.* (2021) Co-condensation between transcription factor and coactivator p300 modulates transcriptional bursting kinetics. *Mol Cell*, **81**, 1682-1697.e7.

9. Du,M., Stitzinger,S.H., Spille,J.-H., Cho,W.-K., *et al.* (2024) Direct observation of a condensate effect on super-enhancer controlled gene bursting. *Cell*, 10.1016/j.cell.2023.12.005.

10. Guo,Y.E., Manteiga,J.C., Henninger,J.E., Sabari,B.R., *et al.* (2019) Pol II phosphorylation regulates a switch between transcriptional and splicing condensates. *Nature*, **572**, 543–548.

11. Strom,A.R., Eeftens,J.M., Polyachenko,Y., Weaver,C.J., *et al.* (2024) Interplay of condensation and chromatin binding underlies BRD4 targeting. *Mol Biol Cell*, **35**.

12. Zhang,Y., Brown,K., Yu,Y., Ibrahim,Z., *et al.* (2021) Nuclear condensates of p300 formed though the structured catalytic core can act as a storage pool of p300 with reduced HAT activity. *Nat Commun*, **12**, 4618.

13. Whyte,W.A., Orlando,D.A., Hnisz,D., Abraham,B.J., *et al.* (2013) Master Transcription Factors and Mediator Establish Super-Enhancers at Key Cell Identity Genes. *Cell*, **153**, 307–319.

14. Lovén,J., Hoke,H.A., Lin,C.Y., Lau,A., *et al.* (2013) Selective inhibition of tumor oncogenes by disruption of super-enhancers. *Cell*, **153**, 320–34.

15. Boeva,V., Louis-Brennetot,C., Peltier,A., Durand,S., *et al.* (2017) Heterogeneity of neuroblastoma cell identity defined by transcriptional circuitries. *Nat Genet*, **49**, 1408–1413.

16. Perlman,B.S., Burget,N., Zhou,Y., Schwartz,G.W., *et al.* (2024) Enhancer-promoter hubs organize transcriptional networks promoting oncogenesis and drug resistance. *Nat Commun*, **15**, 8070.

17. Murphy,D., Salataj,E., Di Giammartino,D.C., Rodriguez-Hernaez,J., *et al.* (2024) 3D Enhancer–promoter networks provide predictive features for gene expression and coregulation in early embryonic lineages. *Nat Struct Mol Biol*, **31**, 125–140.

18. The ENCODE Project Consortium (2012) An integrated encyclopedia of DNA elements in the human genome. *Nature*, **489**, 57–74.

19. Carey,M. (1998) The Enhanceosome and Transcriptional Synergy. *Cell*, **92**, 5–8.

20. Levine,M. and Tjian,R. (2003) Transcription regulation and animal diversity. *Nature*, **424**, 147–151.

21. Pombo,A. and Dillon,N. (2015) Three-dimensional genome architecture: players and mechanisms. *Nat Rev Mol Cell Biol*, **16**, 245–257.

22. Shen,Y., Yue,F., McCleary,D.F., Ye,Z., *et al.* (2012) A map of the cis-regulatory sequences in the mouse genome. *Nature*, **488**, 116–120.

23. Visel,A., Rubin,E.M. and Pennacchio,L.A. (2009) Genomic views of distant-acting enhancers. *Nature*, **461**, 199–205.

24. Williamson,I., Hill,R.E. and Bickmore,W.A. (2011) Enhancers: From Developmental Genetics to the Genetics of Common Human Disease. *Dev Cell*, **21**, 17–19.

25. Di Giammartino,D.C., Kloetgen,A., Polyzos,A., Liu,Y., *et al.* (2019) KLF4 is involved in the organization and regulation of pluripotency-associated three-dimensional enhancer networks. *Nat Cell Biol*, **21**, 1179–1190.

26. Oudelaar,A.M., Davies,J.O.J., Hanssen,L.L.P., Telenius,J.M., *et al.* (2018) Single-allele chromatin interactions identify regulatory hubs in dynamic compartmentalized domains. *Nat Genet*, **50**, 1744–1751.

27. Lim,B. and Levine,M.S. (2021) Enhancer-promoter communication: hubs or loops? *Curr Opin Genet Dev*, **67**, 5–9.

28. Madsen,J.G.S., Madsen,M.S., Rauch,A., Traynor,S., *et al.* (2020) Highly interconnected enhancer communities control lineage-determining genes in human mesenchymal stem cells. *Nat Genet*, **52**, 1227–1238.

29. Talukdar,P.D. and Chatterji,U. (2023) Transcriptional co-activators: emerging roles in signaling pathways and potential therapeutic targets for diseases. *Signal Transduct Target Ther*, **8**, 427.

30. Tsai,A., Alves,M.R. and Crocker,J. (2019) Multi-enhancer transcriptional hubs confer phenotypic robustness. *Elife*, **8**.

31. Uyehara,C.M. and Apostolou,E. (2023) 3D enhancer-promoter interactions and multi-connected hubs: Organizational principles and functional roles. *Cell Rep*, **42**, 112068.

32. Miguel-Escalada,I., Bonàs-Guarch,S., Cebola,I., Ponsa-Cobas,J., *et al.* (2019) Human pancreatic islet three-dimensional chromatin architecture provides insights into the genetics of type 2 diabetes. *Nat Genet*, **51**, 1137–1148.

33. Serfling,E., Lübbe,A., Dorsch-Häsler,K. and Schaffner,W. (1985) Metal-dependent SV40 viruses containing inducible enhancers from the upstream region of metallothionein genes. *EMBO J*, **4**, 3851–3859.

34. Nguyen,T.A., Jones,R.D., Snavely,A.R., Pfenning,A.R., *et al.* (2016) High-throughput functional comparison of promoter and enhancer activities. *Genome Res*, **26**, 1023–33.

35. Dowen,J.M., Fan,Z.P., Hnisz,D., Ren,G., *et al.* (2014) Control of Cell Identity Genes Occurs in Insulated Neighborhoods in Mammalian Chromosomes. *Cell*, **159**, 374–387.

36. Ji,X., Dadon,D.B., Powell,B.E., Fan,Z.P., *et al.* (2016) 3D Chromosome Regulatory Landscape of Human Pluripotent Cells. *Cell Stem Cell*, **18**, 262–275.

37. Hnisz,D., Day,D.S. and Young,R.A. (2016) Insulated Neighborhoods: Structural and Functional Units of Mammalian Gene Control. *Cell*, **167**, 1188–1200.

38. Kohrt,S.E., Novak,E.J., Tapadar,S., Wu,B., *et al.* (2024) Small-molecule disruption of androgen receptor–dependent chromatin clusters. *Proceedings of the National Academy of Sciences*, **121**.

39. Hnisz,D., Abraham,B.J., Lee,T.I., Lau,A., *et al.* (2013) Super-enhancers in the control of cell identity and disease. *Cell*, **155**, 934–47.

40. Dixon,J.R., Selvaraj,S., Yue,F., Kim,A., *et al.* (2012) Topological domains in mammalian genomes identified by analysis of chromatin interactions. *Nature*, **485**, 376–380.

41. Csardi,G. and Nepusz,T. (2006) The igraph software package for complex network research. *InterJournal*, **Complex Systems**, 1695.

42. Fortunato,S. (2010) Community detection in graphs. *Phys Rep*, **486**, 75–174.

43. Raghavan,U.N., Albert,R. and Kumara,S. (2007) Near linear time algorithm to detect community structures in large-scale networks. *Phys Rev E*, **76**, 036106.

44. Ulianov,S. V., Khrameeva,E.E., Gavrilov,A.A., Flyamer,I.M., *et al.* (2016) Active chromatin and transcription play a key role in chromosome partitioning into topologically associating domains. *Genome Res*, **26**, 70–84.

45. Rao,S.S.P., Huntley,M.H., Durand,N.C., Stamenova,E.K., *et al.* (2014) A 3D Map of the Human Genome at Kilobase Resolution Reveals Principles of Chromatin Looping. *Cell*, **159**, 1665–1680.

46. Sexton,T., Yaffe,E., Kenigsberg,E., Bantignies,F., *et al.* (2012) Three-Dimensional Folding and Functional Organization Principles of the Drosophila Genome. *Cell*, **148**, 458–472.

47. Huang,J., Li,K., Cai,W., Liu,X., *et al.* (2018) Dissecting super-enhancer hierarchy based on chromatin interactions. *Nat Commun*, **9**, 943.

48. McCord,R.P., Kaplan,N. and Giorgetti,L. (2020) Chromosome Conformation Capture and Beyond: Toward an Integrative View of Chromosome Structure and Function. *Mol Cell*, **77**, 688–708.

49. Chen,Z., Ye,Z., Soccio,R.E., Nakadai,T., *et al.* (2022) Phosphorylated MED1 links transcription recycling and cancer growth. *Nucleic Acids Res*, **50**, 4450–4463.

50. Buenrostro,J.D., Wu,B., Chang,H.Y. and Greenleaf,W.J. (2015) ATAC-seq: A Method for Assaying Chromatin Accessibility Genome-Wide. *Curr Protoc Mol Biol*, **109**.

51. Wu,C. (1980) The 5′ ends of Drosophila heat shock genes in chromatin are hypersensitive to DNase I. *Nature*, **286**, 854–860.

52. Stalder,J., Larsen,A., Engel,J., Dolan,M. and Weintraub,H. (1980) Tissue-specific DNA cleavages in the globin chromatin domain introduced by DNAase I. *Cell*, **20**, 451–460.

53. Zhang,S. (2014) Sox2, a key factor in the regulation of pluripotency and neural differentiation. *World J Stem Cells*, **6**, 305.

54. Boyer,L.A., Lee,T.I., Cole,M.F., Johnstone,S.E., *et al.* (2005) Core transcriptional regulatory circuitry in human embryonic stem cells. *Cell*, **122**, 947–56.

55. Takahashi,K. and Yamanaka,S. (2006) Induction of pluripotent stem cells from mouse embryonic and adult fibroblast cultures by defined factors. *Cell*, **126**, 663–76.

56. Buganim,Y., Markoulaki,S., van Wietmarschen,N., Hoke,H., *et al.* (2014) The developmental potential of iPSCs is greatly influenced by reprogramming factor selection. *Cell Stem Cell*, **15**, 295–309.

57. Zhou,H.Y., Katsman,Y., Dhaliwal,N.K., Davidson,S., *et al.* (2014) A Sox2 distal enhancer cluster regulates embryonic stem cell differentiation potential. *Genes Dev*, **28**, 2699–711.

58. Liu,Z., Legant,W.R., Chen,B.-C., Li,L., *et al.* (2014) 3D imaging of Sox2 enhancer clusters in embryonic stem cells. *Elife*, **3**.

59. Li,Y., Rivera,C.M., Ishii,H., Jin,F., *et al.* (2014) CRISPR Reveals a Distal Super-Enhancer Required for Sox2 Expression in Mouse Embryonic Stem Cells. *PLoS One*, **9**, e114485.

60. Medeiros,L.A., Dennis,L.M., Gill,M.E., Houbaviy,H., *et al.* (2011) *Mir-290–295* deficiency in mice results in partially penetrant embryonic lethality and germ cell defects. *Proceedings of the National Academy of Sciences*, **108**, 14163–14168.

61. Hnisz,D., Schuijers,J., Lin,C.Y., Weintraub,A.S., *et al.* (2015) Convergence of Developmental and Oncogenic Signaling Pathways at Transcriptional Super-Enhancers. *Mol Cell*, **58**, 362–370.

62. Fulco,C.P., Nasser,J., Jones,T.R., Munson,G., *et al.* (2019) Activity-by-contact model of enhancer-promoter regulation from thousands of CRISPR perturbations. *Nat Genet*, **51**, 1664–1669.

63. Sun,F., Sun,T., Kronenberg,M., Tan,X., *et al.* (2021) The Pol II preinitiation complex (PIC) influences Mediator binding but not promoter-enhancer looping. *Genes Dev*, **35**, 1175–1189.

64. Zabidi,M.A., Arnold,C.D., Schernhuber,K., Pagani,M., *et al.* (2015) Enhancer-core-promoter specificity separates developmental and housekeeping gene regulation. *Nature*, **518**, 556–9.

65. Zhang,Y., Brown,K., Yu,Y., Ibrahim,Z., *et al.* (2021) Nuclear condensates of p300 formed though the structured catalytic core can act as a storage pool of p300 with reduced HAT activity. *Nat Commun*, **12**, 4618.

66. Creyghton,M.P., Cheng,A.W., Welstead,G.G., Kooistra,T., *et al.* (2010) Histone H3K27ac separates active from poised enhancers and predicts developmental state. *Proceedings of the National Academy of Sciences*, **107**, 21931–21936.

67. Dejosez,M., Krumenacker,J.S., Zitur,L.J., Passeri,M., *et al.* (2008) Ronin Is Essential for Embryogenesis and the Pluripotency of Mouse Embryonic Stem Cells. *Cell*, **133**, 1162–1174.

68. Dejosez,M., Dall'Agnese,A., Ramamoorthy,M., Platt,J., *et al.* (2023) Regulatory architecture of housekeeping genes is driven by promoter assemblies. *Cell Rep*, **42**, 112505.

69. Zhou,R., Tian,K., Huang,J., Duan,W., *et al.* (2022) CTCF DNA-binding domain undergoes dynamic and selective protein-protein interactions. *iScience*, **25**, 105011.

70. Zamudio,A. V, Dall'Agnese,A., Henninger,J.E., Manteiga,J.C., *et al.* (2019) Mediator Condensates Localize Signaling Factors to Key Cell Identity Genes. *Mol Cell*, **76**, 753-766.e6.

71. Geisler,M.S., Kemp,J.P. and Duronio,R.J. (2023) Histone locus bodies: a paradigm for how nuclear biomolecular condensates control cell cycle regulated gene expression. *Nucleus*, **14**, 2293604.

72. Zhou,P., VanDusen,N.J., Zhang,Y., Cao,Y., *et al.* (2023) Dynamic changes in P300 enhancers and enhancer-promoter contacts control mouse cardiomyocyte maturation. *Dev Cell*, **58**, 898-914.e7.

73. Stroud,H., Yang,M.G., Tsitohay,Y.N., Davis,C.P., *et al.* (2020) An Activity-Mediated Transition in Transcription in Early Postnatal Neurons. *Neuron*, **107**, 874-890.e8.

74. Zelenka,T., Klonizakis,A., Tsoukatou,D., Papamatheakis,D.-A., *et al.* (2022) The 3D enhancer network of the developing T cell genome is shaped by SATB1. *Nat Commun*, **13**, 6954.

75. Van Gool,F., Nguyen,M.L.T., Mumbach,M.R., Satpathy,A.T., *et al.* (2019) A Mutation in the Transcription Factor Foxp3 Drives T Helper 2 Effector Function in Regulatory T Cells. *Immunity*, **50**, 362-377.e6.

76. Mammadli,M., Harris,R., Suo,L., May,A., *et al.* (2021) Interleukin-2-inducible T-cell kinase (Itk) signaling regulates potent noncanonical regulatory T cells. *Clin Transl Med*, **11**.

77. Kioussis,D. and Ellmeier,W. (2002) Chromatin and CD4, CD8A and CD8B gene expression during thymic differentiation. *Nat Rev Immunol*, **2**, 909–919.

78. Blankvoort,S., Olsen,L.C. and Kentros,C.G. (2022) Single Cell Transcriptomic and Chromatin Profiles Suggest Layer Vb Is the Only Layer With Shared Excitatory Cell Types in the Medial and Lateral Entorhinal Cortex. *Front Neural Circuits*, **15**.

79. Galdos,F.X., Lee,C. and Wu,S.M. (2024) Cardiac ACTN2 enhancer regulates cardiometabolism and maturation. *Nature Cardiovascular Research*, **3**, 616–618.

80. Vogiatzoglou,A.P., Moretto,F., Makkou,M., Papamatheakis,J. and Kretsovali,A. (2022) Promyelocytic leukemia protein (PML) and stem cells: from cancer to pluripotency. *Int J Dev Biol*, **66**, 85–95.

81. Cole,M.F., Johnstone,S.E., Newman,J.J., Kagey,M.H. and Young,R.A. (2008) Tcf3 is an integral component of the core regulatory circuitry of embryonic stem cells. *Genes Dev*, **22**, 746–55.

82. Martello,G., Bertone,P. and Smith,A. (2013) Identification of the missing pluripotency mediator downstream of leukaemia inhibitory factor. *EMBO J*, **32**, 2561–74.

83. Mullen,A.C., Orlando,D.A., Newman,J.J., Lovén,J., *et al.* (2011) Master transcription factors determine cell-type-specific responses to TGF-β signaling. *Cell*, **147**, 565–76.

84. Wang,Z., Zhang,Z., Luo,S., Zhou,T. and Zhang,J. (2024) Power-law behavior of transcriptional bursting regulated by enhancer-promoter communication. *Genome Res*, **34**, 106–118.

85. Huang,J., Li,K., Cai,W., Liu,X., *et al.* (2018) Dissecting super-enhancer hierarchy based on chromatin interactions. *Nat Commun*, **9**, 943.

86. Panigrahi,A. and O'Malley,B.W. (2021) Mechanisms of enhancer action: the known and the unknown. *Genome Biol*, **22**, 108.

87. Ebisuya,M., Yamamoto,T., Nakajima,M. and Nishida,E. (2008) Ripples from neighbouring transcription. *Nat Cell Biol*, **10**, 1106–1113.

Figure 1

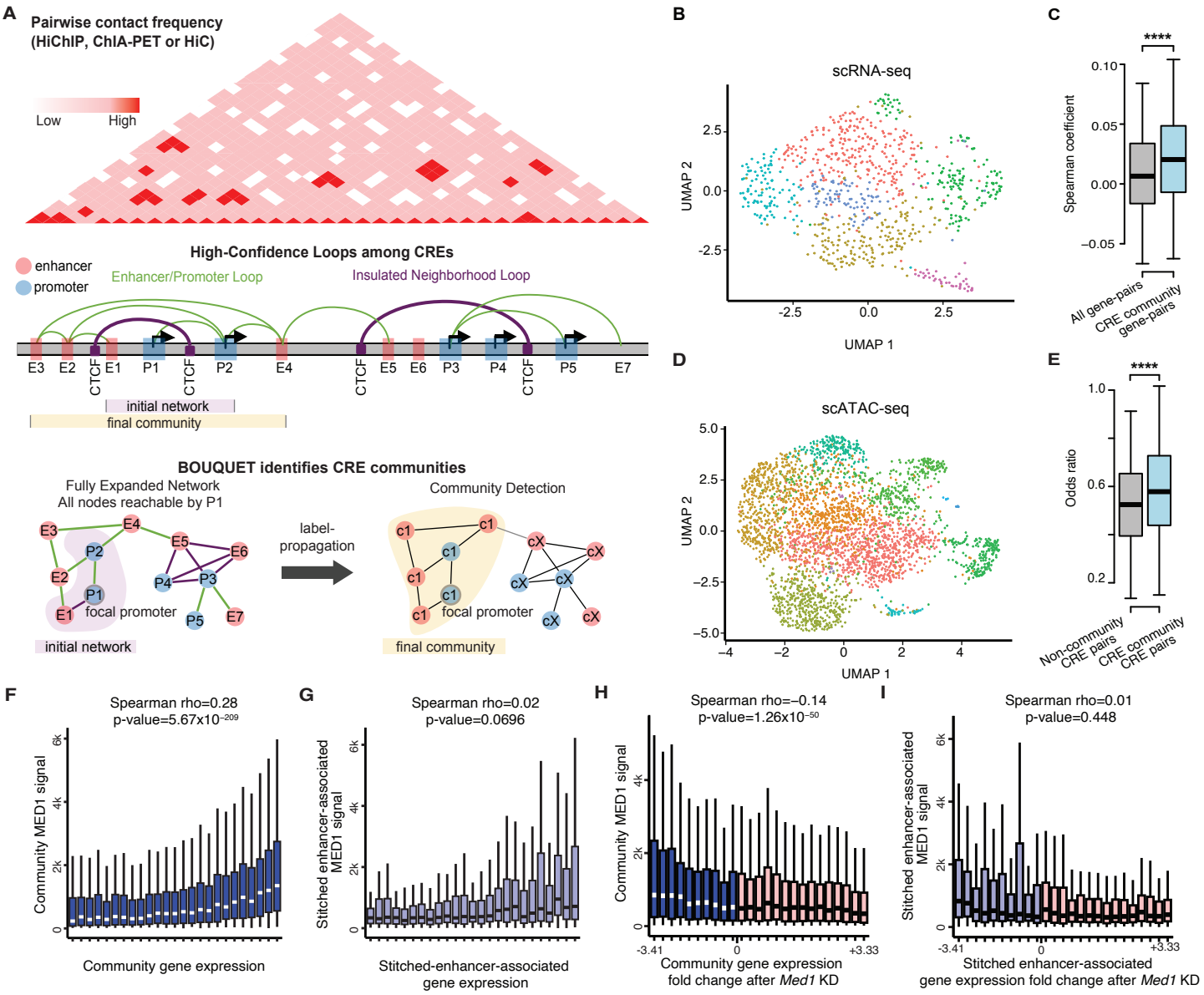
A
Pairwise contact frequency
(HiChIP, ChIA-PET or HiC)
Low
High
High-Confidence Loops among CREs
enhancer
promoter
Enhancer/Promoter Loop
Insulated Neighborhood Loop
E3 E2 CTCF E1 P1 CTCF P2 E4 CTCF E5 E6 P3 P4 CTCF P5 E7
initial network
final community
BOUQUET identifies CRE communities
Fully Expanded Network
All nodes reachable by P1
focal promoter
initial network
label-propagation
Community Detection
focal promoter
final community
B
scRNA-seq
UMAP 2
UMAP 1
C
****
Spearman coefficient
All gene-pairs
CRE community gene-pairs
D
scATAC-seq
UMAP 2
UMAP 1
E
****
Odds ratio
Non-community CRE pairs
CRE community CRE pairs
F
Spearman rho=0.28
p-value=5.67x10−209
Community MED1 signal
Community gene expression
G
Spearman rho=0.02
p-value=0.0696
Stitched enhancer-associated MED1 signal
Stitched-enhancer-associated gene expression
H
Spearman rho=−0.14
p-value=1.26x10−50
Community MED1 signal
Community gene expression fold change after Med1 KD
I
Spearman rho=0.01
p-value=0.448
Stitched enhancer-associated MED1 signal
Stitched enhancer-associated gene expression fold change after Med1 KD

Figure 1: BOUQUET identifies cis-regulatory element communities and uncovers relationships between accumulated protein apparatus and gene expression. (**A**) Workflow of Building Optimized Units of Quantified Enhancer Topologies (BOUQUET). High-confidence loops between CRE-pairs (green) are identified by H3K27ac HiChIP using the Hi-LOW pipeline (see Supplemental Methods). Interactions between pairs of CTCF binding sites that are also bound by cohesin form Insulated Neighborhoods (IN) (purple) and are used by BOUQUET to connect CRE-pairs. CRE-pairs are assembled into an initial CRE network. Using label-propagation, BOUQUET identifies a focal gene's CRE community by uncovering densely interconnected subnetworks (highlighted in yellow). See Methods for additional details. (**B**) UMAP plot of scRNA-seq in 847 mESCs. Colors represent Seurat-derived clusters. (**C**) Distributions of the Spearman's correlation coefficient calculated from scRNA-seq data for the co-expression of gene-pairs from two categories: genome-wide control (gray, median r= 0.0065) and gene-pairs within the same CRE community (blue, median r=0.02), p-value < 2.0×10^{-308} (Wilcoxon Rank Sum Test, Supplemental Methods). Whiskers represent interquartile range. (**D**) UMAP plot of scATAC-seq in 3,171 mESCs. Colors represent Seurat-derived clusters. (**E**) Distributions of the odds ratio calculated from scATAC-seq data for the co-accessibility of CRE-pairs from two categories: genome-wide control, i.e., not within the same CRE community (gray, median odds ratio (OR)=0.52) and CRE-pairs within the same CRE community (blue, median OR=0.58, p-value $=1.6 \times 10^{-25}$ (bootstrapping procedure assuming normal distribution). Whisker length represents interquartile range. (**F**) Distributions of community-assigned per-gene MED1 signal across grouped genes. Genes are sorted into 25 groups by increasing expression level. (**G**) Distributions of ROSE-assigned per-stitched-enhancer-associated gene MED1 signal, arranged into 25 groups by increasing gene expression level. (**H**) Distributions of community-assigned per-gene MED1 signal across grouped genes following knockdown of *Med1*. Genes are sorted into 25 groups by their expression fold-change after *Med1* knock-down. Blue indicates downregulation of community gene expression following *Med1* KD; pink indicates upregulation of community gene expression following *Med1* KD. (**I**) Distributions of ROSE-assigned per-stitched-enhancer-associated gene MED1 signal following knock-down of *Med1*. Genes are sorted into 25 groups by their expression fold-change after *Med1* knock-down. Blue indicates downregulation of stitched enhancer-associated gene expression following *Med1* KD; pink indicates upregulation of stitched enhancer-associated gene expression following *Med1* KD.

Figure 2

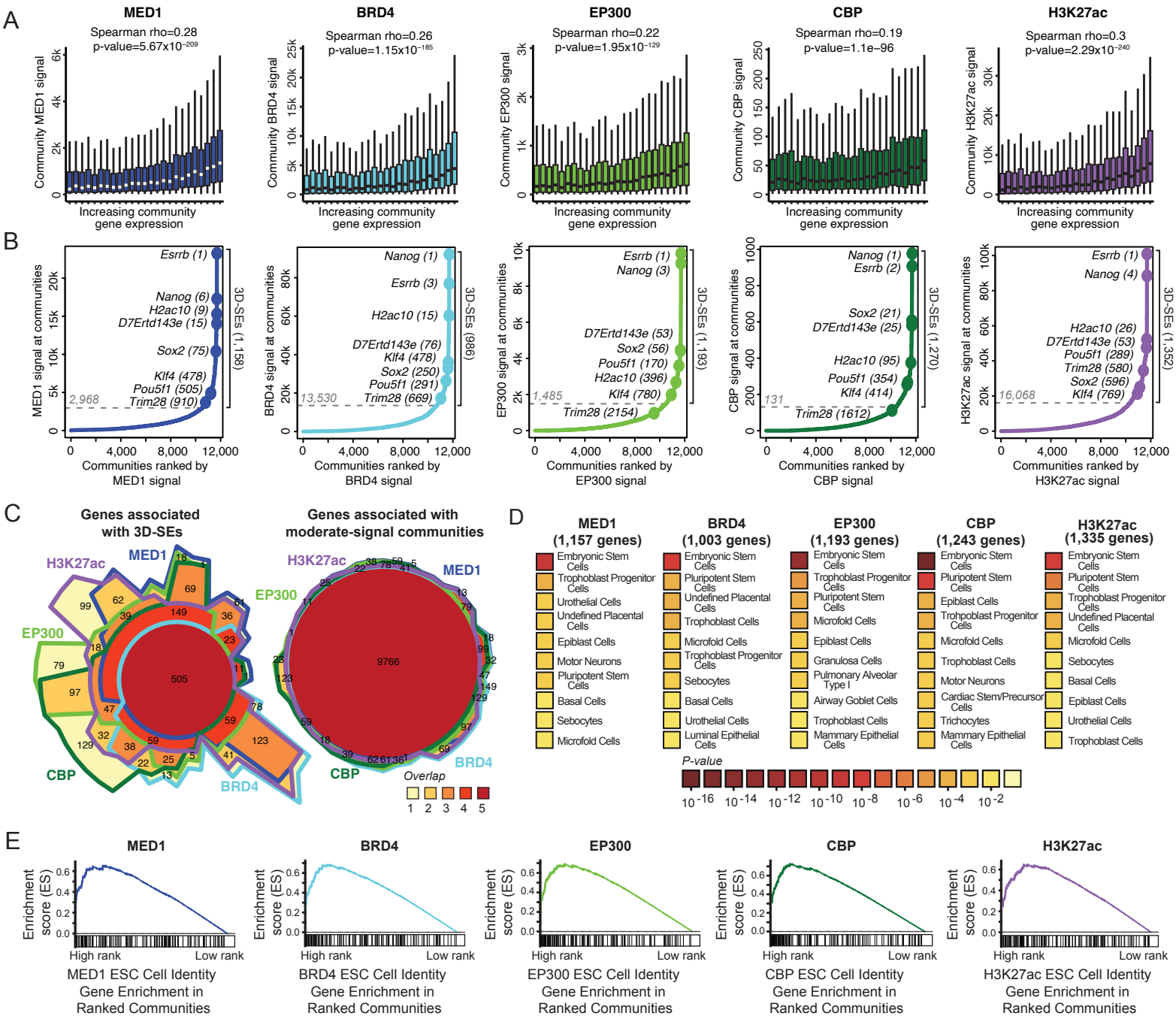
A
MED1
Spearman rho=0.28
p-value=5.67x10-209
Community MED1 signal
BRD4
Spearman rho=0.26
p-value=1.15x10-185
Community BRD4 signal
EP300
Spearman rho=0.22
p-value=1.95x10-129
Community EP300 signal
CBP
Spearman rho=0.19
p-value=1.1e-96
Community CBP signal
H3K27ac
Spearman rho=0.3
p-value=2.29x10-240
Community H3K27ac signal
Increasing community gene expression
B
MED1 signal at communities
Esrrb (1)
Nanog (6)
H2ac10 (9)
D7Ertd143e (15)
Sox2 (75)
Klf4 (478)
Pou5f1 (505)
Trim28 (910)
2,968
3D-SEs (1,158)
Communities ranked by MED1 signal
BRD4 signal at communities
Nanog (1)
Esrrb (3)
H2ac10 (15)
D7Ertd143e (76)
Klf4 (478)
Sox2 (250)
Pou5f1 (291)
Trim28 (669)
13,530
3D-SEs (986)
Communities ranked by BRD4 signal
EP300 signal at communities
Esrrb (1)
Nanog (3)
D7Ertd143e (53)
Sox2 (56)
Pou5f1 (170)
H2ac10 (396)
Klf4 (780)
Trim28 (2154)
1,485
3D-SEs (1,193)
Communities ranked by EP300 signal
CBP signal at communities
Nanog (1)
Esrrb (2)
Sox2 (21)
D7Ertd143e (25)
H2ac10 (95)
Pou5f1 (354)
Klf4 (414)
Trim28 (1612)
131
3D-SEs (1,270)
Communities ranked by CBP signal
H3K27ac signal at communities
Esrrb (1)
Nanog (4)
H2ac10 (26)
D7Ertd143e (53)
Pou5f1 (289)
Trim28 (580)
Sox2 (596)
Klf4 (769)
16,068
3D-SEs (1,352)
Communities ranked by H3K27ac signal
C
Genes associated with 3D-SEs
Genes associated with moderate-signal communities
H3K27ac
MED1
EP300
CBP
BRD4
505
9766
Overlap
1 2 3 4 5
D
MED1 (1,157 genes)
Embryonic Stem Cells
Trophoblast Progenitor Cells
Urothelial Cells
Undefined Placental Cells
Epiblast Cells
Motor Neurons
Pluripotent Stem Cells
Basal Cells
Sebocytes
Microfold Cells
BRD4 (1,003 genes)
Embryonic Stem Cells
Pluripotent Stem Cells
Undefined Placental Cells
Trophoblast Cells
Microfold Cells
Trophoblast Progenitor Cells
Sebocytes
Basal Cells
Urothelial Cells
Luminal Epithelial Cells
EP300 (1,193 genes)
Embryonic Stem Cells
Trophoblast Progenitor Cells
Pluripotent Stem Cells
Microfold Cells
Epiblast Cells
Granulosa Cells
Pulmonary Alveolar Type I
Airway Goblet Cells
Trophoblast Cells
Mammary Epithelial Cells
CBP (1,243 genes)
Embryonic Stem Cells
Pluripotent Stem Cells
Epiblast Cells
Trohpoblast Progenitor Cells
Microfold Cells
Trophoblast Cells
Motor Neurons
Cardiac Stem/Precursor Cells
Trichocytes
Mammary Epithelial Cells
H3K27ac (1,335 genes)
Embryonic Stem Cells
Pluripotent Stem Cells
Trophoblast Progenitor Cells
Undefined Placental Cells
Microfold Cells
Sebocytes
Basal Cells
Epiblast Cells
Urothelial Cells
Trophoblast Cells
P-value
10-16 10-14 10-12 10-10 10-8 10-6 10-4 10-2
E
MED1
BRD4
EP300
CBP
H3K27ac
Enrichment score (ES)
High rank
Low rank
MED1 ESC Cell Identity Gene Enrichment in Ranked Communities
BRD4 ESC Cell Identity Gene Enrichment in Ranked Communities
EP300 ESC Cell Identity Gene Enrichment in Ranked Communities
CBP ESC Cell Identity Gene Enrichment in Ranked Communities
H3K27ac ESC Cell Identity Gene Enrichment in Ranked Communities

Figure 2: Ranking communities by co-activator binding reveals 3D super-enhancers. (**A**) Cumulative per-community signal versus focal gene expression level for MED1, BRD4, EP300, CBP, or H3K27ac. The MED1 panel is duplicated from Fig. 1F and is provided here for ease of comparison. (**B**) Distribution of signal ranking across CRE communities for each of four co-activators and H3K27ac. X-axis is the signal rank of community; Y-axis is the summed signal amount at the CREs of each community. Example known condensate-associated genes are highlighted. The number of 3D-SEs is shown on the right. The algorithmically determined signal cutoff that distinguishes 3D-SEs is noted by the dashed line. (**C**) Chow-Ruskey diagrams showing the area-proportional overlap of genes associated with 3D-SEs (left) and moderate-signal communities (right) for four co-activators and H3K27ac. (**D**) Gene ontology analysis for cell type term enrichment in 3D-SE genes ranked by one of four co-activators or H3K27ac. The top 10 most enriched terms from the PanglaoDB_Augmented_2021 database are shown for each factor (Supplemental Methods). (**E**) Pre-ranked gene set enrichment analysis (GSEA) for mESC cell identity genes across communities ranked for each of four co-activators and H3K27ac. Rank by community signal was compared to the "Embryonic Stem Cell" gene list from the PanglaoDB_Augmented_2021 database (Supplemental Methods).

Figure 3

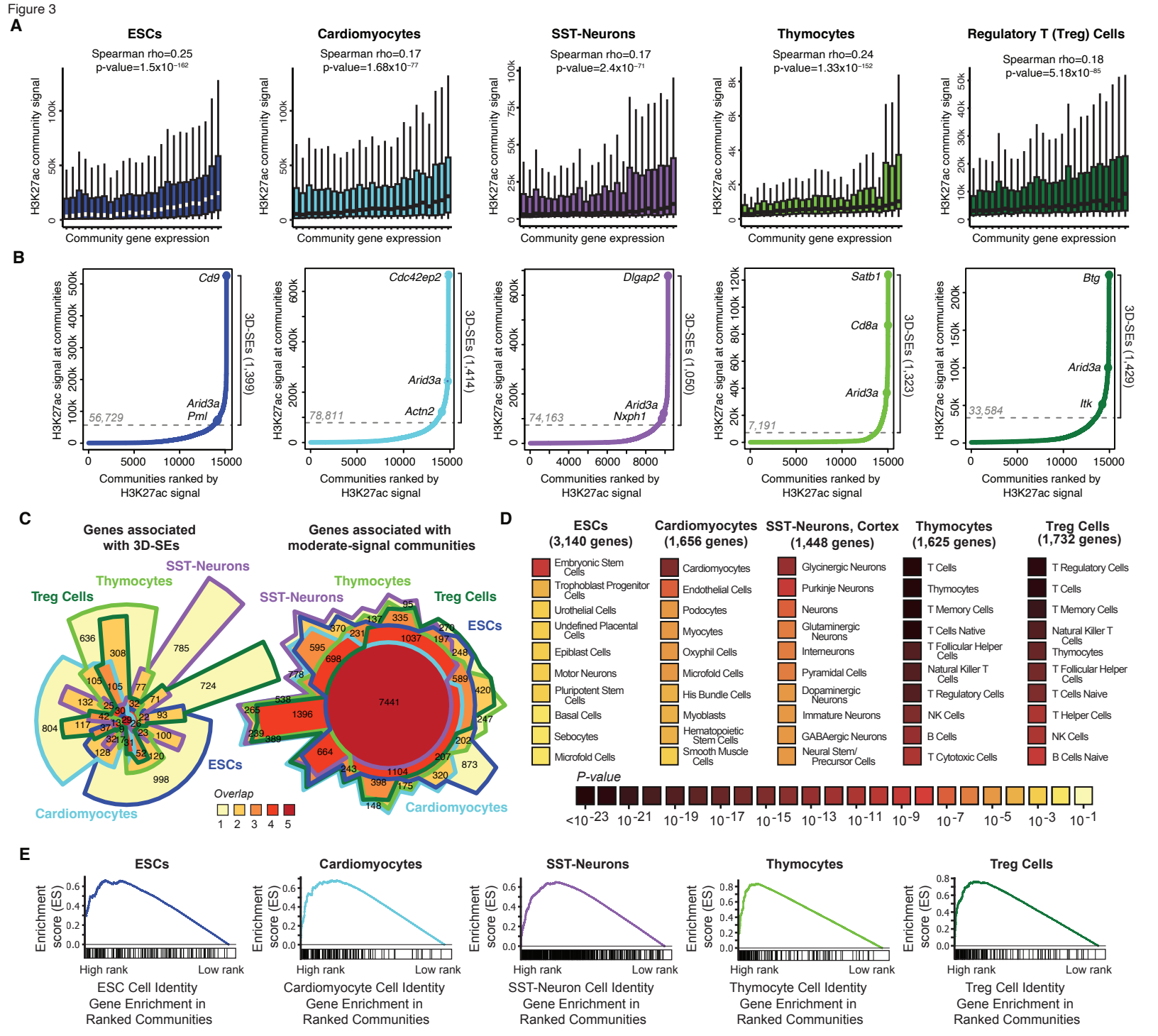
A
ESCs
Spearman rho=0.25
p-value=1.5x10-162
Cardiomyocytes
Spearman rho=0.17
p-value=1.68x10-77
SST-Neurons
Spearman rho=0.17
p-value=2.4x10-71
Thymocytes
Spearman rho=0.24
p-value=1.33x10-152
Regulatory T (Treg) Cells
Spearman rho=0.18
p-value=5.18x10-85
H3K27ac community signal
Community gene expression
B
H3K27ac signal at communities
Communities ranked by H3K27ac signal
Cd9
Arid3a
Pml
56,729
3D-SEs (1,399)
Cdc42ep2
Arid3a
Actn2
78,811
3D-SEs (1,414)
Dlgap2
Arid3a
Nxph1
74,163
3D-SEs (1,050)
Satb1
Cd8a
Arid3a
7,191
3D-SEs (1,323)
Btg
Arid3a
Itk
33,584
3D-SEs (1,429)
C
Genes associated with 3D-SEs
Genes associated with moderate-signal communities
SST-Neurons
Thymocytes
Treg Cells
ESCs
Cardiomyocytes
Overlap
1 2 3 4 5
D
ESCs (3,140 genes)
Embryonic Stem Cells
Trophoblast Progenitor Cells
Urothelial Cells
Undefined Placental Cells
Epiblast Cells
Motor Neurons
Pluripotent Stem Cells
Basal Cells
Sebocytes
Microfold Cells
Cardiomyocytes (1,656 genes)
Cardiomyocytes
Endothelial Cells
Podocytes
Myocytes
Oxyphil Cells
Microfold Cells
His Bundle Cells
Myoblasts
Hematopoietic Stem Cells
Smooth Muscle Cells
SST-Neurons, Cortex (1,448 genes)
Glycinergic Neurons
Purkinje Neurons
Neurons
Glutaminergic Neurons
Interneurons
Pyramidal Cells
Dopaminergic Neurons
Immature Neurons
GABAergic Neurons
Neural Stem/ Precursor Cells
Thymocytes (1,625 genes)
T Cells
Thymocytes
T Memory Cells
T Cells Native
T Follicular Helper Cells
Natural Killer T Cells
T Regulatory Cells
NK Cells
B Cells
T Cytotoxic Cells
Treg Cells (1,732 genes)
T Regulatory Cells
T Cells
T Memory Cells
Natural Killer T Cells
Thymocytes
T Follicular Helper Cells
T Cells Naive
T Helper Cells
NK Cells
B Cells Naive
P-value
<10-23 10-21 10-19 10-17 10-15 10-13 10-11 10-9 10-7 10-5 10-3 10-1
E
ESCs
Cardiomyocytes
SST-Neurons
Thymocytes
Treg Cells
Enrichment score (ES)
High rank
Low rank
ESC Cell Identity Gene Enrichment in Ranked Communities
Cardiomyocyte Cell Identity Gene Enrichment in Ranked Communities
SST-Neuron Cell Identity Gene Enrichment in Ranked Communities
Thymocyte Cell Identity Gene Enrichment in Ranked Communities
Treg Cell Identity Gene Enrichment in Ranked Communities

Figure 3: 3D-SEs mark cell-identity-defining genes across tissues. (**A**) Cumulative per-community H3K27ac HiChIP signal versus focal gene expression level for five mouse cell and tissue types: mouse embryonic stem cells (mESCs), cardiomyocytes, somatostatin (SST)-producing neurons, thymocytes, and regulatory T (Treg) cells. (**B**) Distribution of signal ranking across CRE communities in five mouse cell and tissue types. X-axis is the H3K27ac HiChIP signal rank of community; Y-axis is the summed H3K27ac HiChIP signal amount at the CREs of each community. Example genes are highlighted, including the highest-ranked gene, a representative cell-identity-defining gene, and a gene called as 3D-SE-associated in all 5 cell types (*Arid3a*). The number of 3D-SEs is shown on the right. The signal cutoff distinguishing 3D-SEs is noted by the dashed line. A minority of communities exceed this 3D-SE threshold in each ell type: 10.2% in mESCs, 10.5% in cardiomyocytes, 7.9% in somatostatin (SST)-expressing neurons, 9.7% in thymocytes, and 10.6% in regulatory T (Treg) cells. (**C**) Chow-Ruskey diagrams showing the area-proportional overlap of genes associated with moderate-signal communities (left) or 3D-SEs (right) in combinations of five cell/tissue types. (**D**) Gene ontology analysis for cell type term enrichment in 3D-SE genes across five cell/tissue types. The top 10 most enriched terms from the PanglaoDB_Augmented _2021 database are shown for each cell/tissue type (Supplemental Methods). (**E**) Pre-ranked gene set enrichment analysis (GSEA) for cell identity genes in five mouse cell and tissue types. Rank by community signal was compared to genes from significantly enriched cell identity terms from the PanglaoDB_Augmented_2021 database (Supplemental Methods).

Figure 4

A

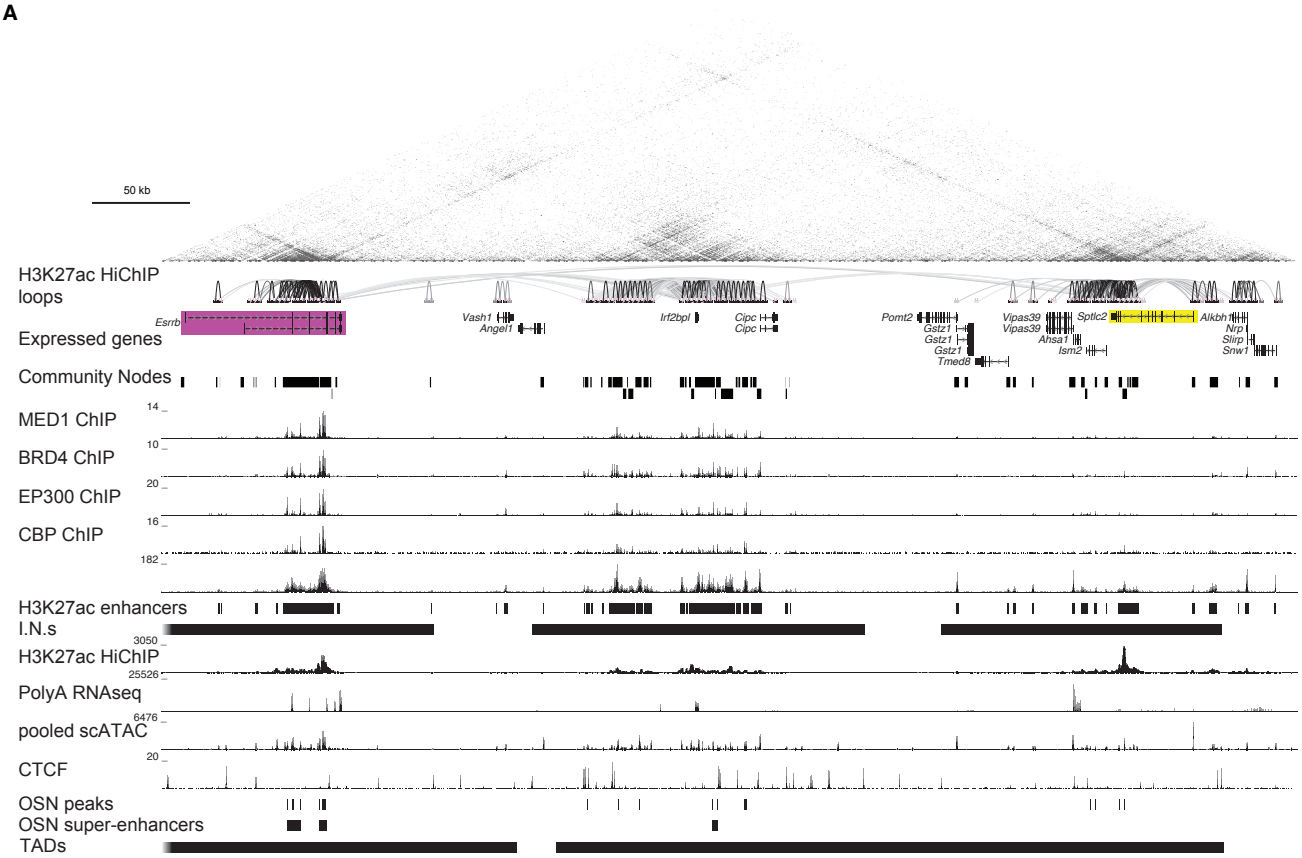

B

DNA FISH + BRD4 IF

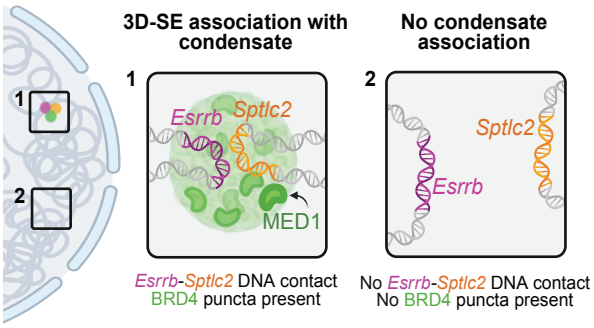

D

Nascent RNA FISH + MED1 EF

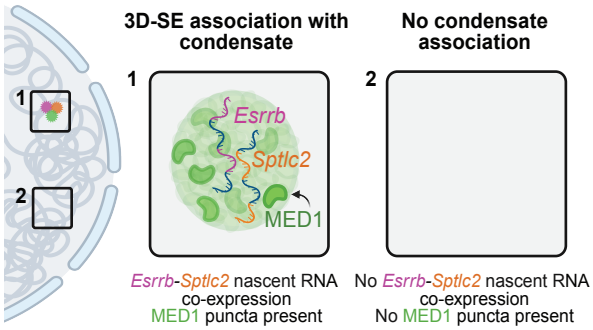

C

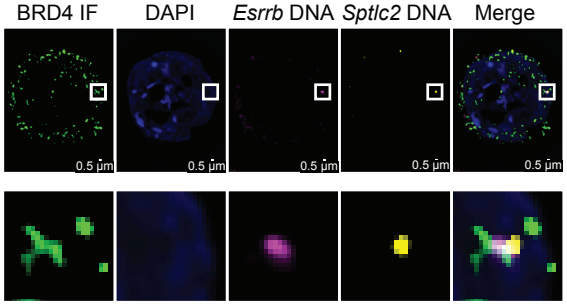

E

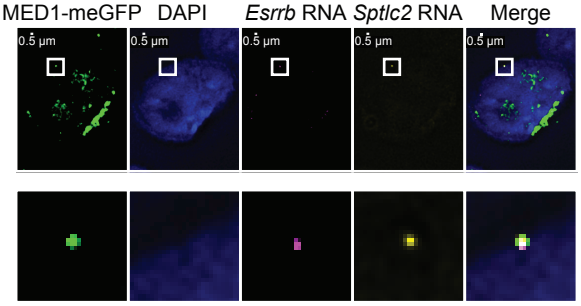

Figure 4: 3D-SEs colocalize with putative co-activator condensates. (**A**) UCSC Genome Browser view of the locus containing the *Esrrb/Irf2bpl/Sptlc2* 3D-SE, the target of the DNA and RNA FISH experiments. (**B**) Model of two predicted outcomes for the DNA FISH and BRD4 immunofluorescence (IF) experiments. In case 1 (*box 1, middle*), the DNAs of two genes are associated within a BRD4 co-activator punctum (*nuclear diagram, left, region of interest (ROI) 1*). In case 2 (*box 2, right*), the DNA are not associated in the ROI (*nuclear diagram, left, ROI 2*). In the model and below, *Esrrb, Sptlc2,* and BRD4 are represented in magenta, yellow and green respectively. Created in BioRender. Maher, K. (2025) https://BioRender.com/fghhosi. **C**) Fluorescence microscopy of mESC nuclei following DNA FISH with BRD4 IF. Blue = DAPI stain for chromatin; magenta = DNA probes for *Esrrb*; yellow = DNA probes for *Sptlc2*; green = anti-BRD4 antibody. Images represent a single z-plane. Scale bar for top panels = 0.5 µm. Lower panels are zoomed-in views of the same ROI shown in the top panels. (**D**) Model of two predicted outcomes for the RNA FISH and endogenously tagged MED1 fluorescence (EF) experiments. In case 1 (*box 1, center*), the mRNAs the two genes encode are associated within a MED1 co-activator punctum (*nuclear diagram, left, ROI 1*). In case 2 (*box 2, right*), the mRNAs are not co-expressed nor associated with MED1 punctum (*nuclear diagram, left, ROI 2*). In the model, *Esrrb, Sptlc2,* and BRD4 are represented in magenta, yellow and green respectively. Created in BioRender. Maher, K. (2025) https://BioRender.com/ycwql9z. (**E**) Fluorescence microscopy of mESC nuclei following RNA FISH with MED1 EF. Blue = DAPI stain for chromatin; magenta = nascent RNA probes for *Esrrb*; yellow = nascent RNA probes for *Sptlc2*; green = MED1 EF. Images represent a single z-plane. Scale bar for top panels = 0.5 µm. Lower panels are zoomed-in views of the same ROI shown in the top panels.